Materials Chemistry and Physics 216 (2018) 508–516

Contents lists available at ScienceDirect

Materials Chemistry and Physics

journal homepage: www.elsevier.com/locate/matchemphys

Supercapacitance and oxygen reduction characteristics of sulfur self-doped micro/mesoporous bio-carbon derived from lignin

Muslum Demir[a,b,*,1], Ahmed A. Farghaly[c,d,1], Matthew J. Decuir[a], Maryanne M. Collinson[e], Ram B. Gupta[a,**]

[a] Department of Chemical and Life Science Engineering, Virginia Commonwealth University, Richmond, VA 23284, United States
[b] Department of Chemical Engineering, Osmaniye Korkut Ata University, Fakuusagı, Osmaniye, Turkey
[c] Advanced Photon Source, Argonne National Laboratory, Argonne, 60439-4854, Illinois, United States
[d] Department of Chemistry, Faculty of Science, Assiut University, 71516, Assiut, Egypt
[e] Department of Chemistry, Virginia Commonwealth University, Richmond, VA 23284, United States

HIGHLIGHTS

- Sulfur-self doped carbon are prepared via a hydrothermal carbonization followed by self-chemical activation.
- Inexpensive and simple manufacturing method.
- High specific capacitance along with durability is achieved.
- The resulting materials show outstanding ORR activity.

GRAPHICAL ABSTRACT

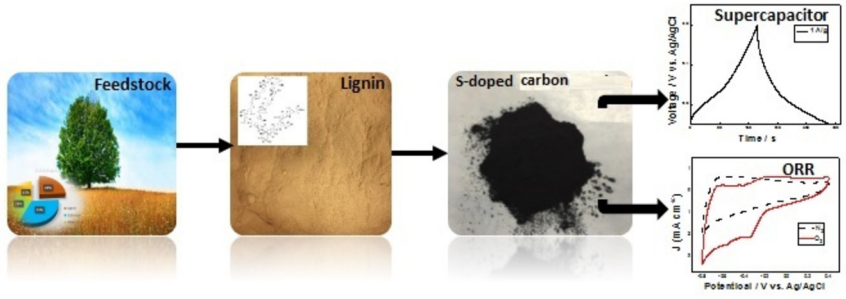

ARTICLE INFO

Keywords:
Supercapacitor
Sulfur-doping
Lignin
Oxygen reduction
Cell
Hydrothermal carbonization

ABSTRACT

The growing global concerns about the increased fossil fuel consumption and related environmental issues have motived scientists to find new, green and sustainable energy resources and technologies. In this work, byproduct lignin biomass was successfully converted into sulfur self-doped carbon via in-situ hydrothermal carbonization followed by thermal annealing. The sulfur surface content in the as-prepared porous carbon is up to 3.2 wt % as indicated by the XPS measurements. Beyond the traditional synthesis methods which employ KOH or $ZnCl_2$ treatment to activate the carbon surface, the developed synthesis strategy doesn't include such separate activation step. Activation of the as-prepared porous carbons has been conducted in-situ via a calcium ions during the synthesis process. The resulting materials displayed high BET surface areas up to 660 $m^2 g^{-1}$ along with micro/meso porosity and graphitic/amorphous carbon structure. The as-prepared sulfur self-doped electrode materials displayed high electrochemical activity for supercapacitor applications. The sulfur-doped carbon SC-850 electrode exhibited capacitance of 225 F/g at a current density of 0.5 A/g, and high durability where the electrode capacitance did not change over 10,000 cycles at harsh conditions. Additionally, the as-prepared sulfur-doped carbons are promising catalysts for oxygen reduction reaction with 3.4 electrons transferred per molecule at 0.8 V, which approaches the optimum 4-electron pathway.

* Corresponding author. Department of Chemical and Life Science Engineering, Virginia Commonwealth University, Richmond, VA 23284, United States.
** Corresponding author.
E-mail addresses: demirm@vcu.edu (M. Demir), rbgupta@vcu.edu (R.B. Gupta).
[1] These authors contributed equally to this work and both should be considered as first author.

https://doi.org/10.1016/j.matchemphys.2018.06.008
Received 20 May 2017; Accepted 3 June 2018
Available online 05 June 2018
0254-0584/

1. Introduction

Electrochemical capacitors (ECs), also called electro-double layer capacitors, are electrochemical devices in which an ion adsorption/desorption process is used to store the charge [1,2]. ECs have attracted a lot of attention over the past decades as potential energy storage devices due to their fast charge/discharge rates and high power density [3] which make them suitable for a wide range of technological applications including hybrid electric vehicles, electronic devices, memory backup etc. Pure electrical double layer capacitors (EDLCs) are based on a non-faradic process to store the charge and exhibit low specific capacitance, which limit their applications and widespread use [4,5]. An appealing route to enhance the capacitance of the EDLCs involves the addition of N, O, S or P heteroatom and/or M_aX_b (where M is a transition metal ion, X is O, S or OH^- and a, b are integers) [6–12]. The add-atom has been designed to enhance the capacitance of a material via storing the charge through a reversible faradic redox reaction [13]. In particular, sulfur has been demonstrated to be an interesting heteroatom dopant of carbon materials for energy storage applications [14,15]. The presence of the sulfur atoms modify the electronic structure and electron density balance of the carbon atoms. As a result, electroactive centers and/or defects are generated on the material surface to enhance the electrocatalytic and capacitive performance of the carbon materials [16–18].

Carbon-based materials such as activated carbon, carbon nanotubes, graphitic carbon, and graphene displayed promising results as electrode material for EDLCs [19]. Traditional methods for the production of porous activated carbon materials include ex-situ treatment of the carbon with chemical agents such as KOH, $ZnCl_2$ or CO_2 to activate the surface. This activation process consume time, money and has the possibility to produce environmental hazards. In this work, activation of the as-prepared porous carbons has been conducted in-situ via a calcium catalyst during the hydrothermal carbonization without the employment of corrosive materials such as KOH or adding extra steps which makes the developed synthesis strategy more environmentally benign, cost and time efficient.

Oxygen reduction reaction (ORR) is an interesting catalytic reaction that has drawn an increasing attention due to its applications in fuel cells, water purification, and metal-air batteries [20–22]. There is a massive effort to develop inexpensive, abundant, chemically stable, highly durable and eco-friendly metal-free ORR catalysts to replace the expensive platinum-based ORR catalysts [23]. Doped carbon materials are fulfilling these requirements and so they are potentials candidates as a metal-free catalysts for the ORR [24].

Among the large number of studies on the application of nitrogen- and sulfur-doped biomass-derived carbon materials in energy storage and fuel cell [25–29], little attention has be devoted toward those derived from lignin biomass [30–36]. Herein, a facile, eco-friendly and scalable synthetic pathway has been developed to produce lignin-derived sulfur self-doped carbon electrodes for use in supercapacitors and oxygen reduction reactions. Impacts of hydrothermal carbonization and thermal annealing on the capacitance of the final material have been studied.

2. Experimental

2.1. Chemicals

Commercially available calcium lignosulfonate (Norlig A) and organosolv (sulfur-free) lignins were received from Lignotech and Lignol Innovations, respectively. Potassium hydroxide (KOH), polytetrafluoroethylene (PTFE, 60 wt% dispersion in H_2O) and 20 wt% Pt/carbon were obtained from Sigma-Aldrich. Carbon black was received from Alfa Aesar. Ni foam was purchased from MTI Corporation. Deionized water (18.2 MΩ cm) was used as a solvent in the hydrothermal carbonizations and the electrochemical measurements.

2.2. Bio-char synthesis from lignin

Bio-char was synthesized via the hydrothermal carbonization (HTC) process [37]. In a typical synthesis, lignin (10 g) was mixed with 80 mL deionized water. The resulting mixture was placed into a 300 mL ultrasonic high-pressure reactor (Col-Int). The reactor is equipped with ultrasonic probe to enhance the mass transfer from the solid phase into the solvent phase and to increase the removal of oxygen from lignin during the hydrothermal treatment [38]. The reaction was carried out at 300°C and 98 bar for 30 min [39]. Water in this reaction was under sub-critical conditions which had both liquid and vapor phases in equilibrium. After the HTC, the reactor was allowed to cool down to ambient temperature. The obtained brown aqueous suspension was filtered to isolate the produced bio-char from the solvent.

2.3. Preparation of sulfur self-doped carbon material from bio-char

Sulfur self-doped carbons were obtained by thermal annealing of the bio-char: 1.0 g of bio-char was charged into a tubular furnace (Carbolite MTF250) and heated to the desired temperature (700–1000 °C) for 1 h under N_2 flow at a heating rate of 5 °C/min. The resulting carbon material was washed with 3 M HCl followed by dilute water in order to remove calcium and other contaminants.

2.4. Physical characterization

Thermogravimetric analysis (TGA) was recorded by a Perkin thermo-gravimetric analyzer with a constant heating rate of 5 °C/min under N_2 flow and temperature ranging from 30 to 1000 °C. FTIR spectra of the as-prepared carbon materials were collected by Nexus 670 FTIR spectrometer which uses a Smart ATR Nicolet. Operating conditions were fixed to average 16 scans at 1 cm^{-1} interval and a resolution of 4 cm^{-1} scanned from 4000 to 400 cm^{-1}. Raman spectra of the carbon materials were collected on Horiba LABRam HR spectroscopy with excitation of 532 nm light source in order to determine degree of graphitization. The morphology of the synthesized materials was examined by scanning electron microscope (SEM, Hitachi SU-70 FE-SEM) at 5 kV acceleration voltage under a vacuum atmosphere. The Brunauer-Emmett-Teller (BET) specific surface area and porosity properties were determined by N_2 adsorption/desorption isotherm with a NOVA surface analyzer. The X-ray photoelectron spectroscopic (XPS) analysis was performed on X-ray photoelectron spectrometer (ESCALAP250) with a monochromatic Al K alpha source (1486.6 eV, 20 kV, 250 W) to determine surface electronic environment of the prepared carbons. The sp^2 carbon peak was adjusted to 284.6 eV to calibrate the XPS energy scale.

2.5. Electrochemical measurements

All electrochemical measurements in this study were performed on a CHI 660E electrochemical workstation (CH Instruments, Inc.) utilizing a conventional three-electrode configuration in 1 M KOH aqueous electrolyte under ambient conditions. Silver/Silver chloride (Ag/AgCl) and platinum wire were used as reference and counter electrodes, respectively. The working electrode was obtained by mixing the active material, carbon black, and PTFE binder with a weight ratio of 80:10:10. The resulting slurry was spread on a nickel foam current collector (1.5 cm × 3 cm) then dried at 80 °C overnight and pressed under a high pressure of 20 MPa. Geometric surface area of 0.32 cm^2 for the working electrode was achieved by using UHMW tape (CS-Hyde). Cyclic voltammetry (CV) measurements were conducted at different constant scan rates (1–100 mV s^{-1}) within the potential window −0.6 to 0.2 V. Galvanostatic charge/discharge measurements were carried out to evaluate the capacitance and cyclability of the as-prepared electrodes at a range of constant current densities (5–20,000 mA/g) between −1.0 and 0.0 V. Electrochemical impedance spectroscopy

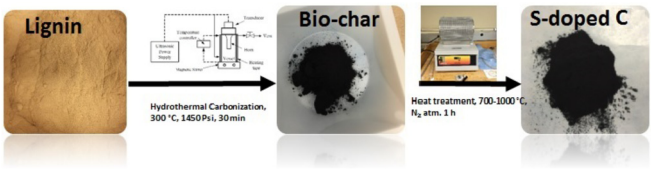

Fig. 1. The synthesis pathway of sulfur self-doped carbons.

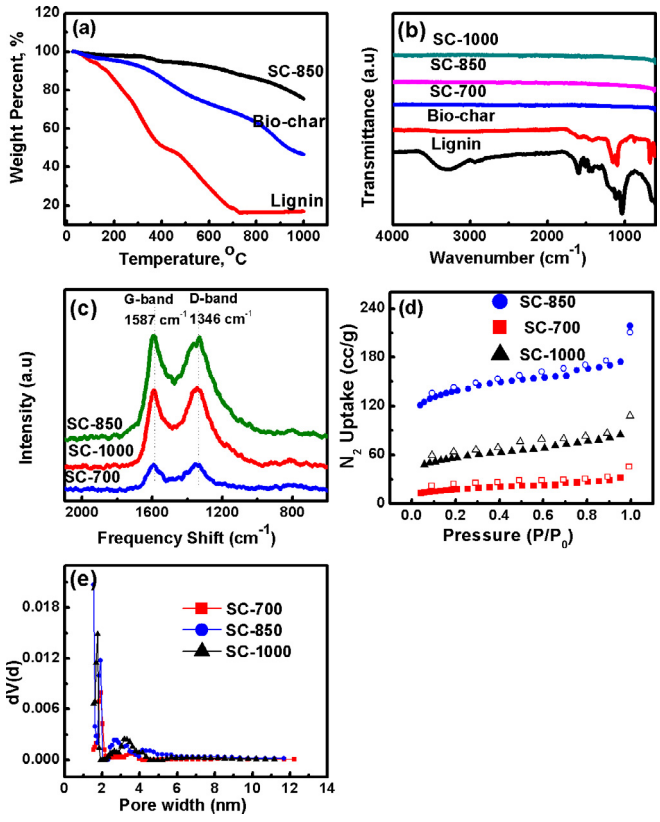

Fig. 2. (a) TGA curves of lignin, bio-char and the as-prepared sulfur self-doped carbon at 850 °C, (b) FTIR spectra of lignin, bio-char and sulfur self-doped carbons, (c) Raman spectra sulfur self-doped carbons, (d) nitrogen uptake at 77 K, (e) pore size distribution calculated from carbon model using adsorption branch fitted, QSDFT.

(EIS) analysis for the supercapacitor electrodes was conducted by applying an AC amplitude of 5 mV within the 10 mHz–0.5 MHz frequency range.

The EIS spectra can be fitted by electrical equivalent circuits, which are composed of R_s, R_{ct}, Zw, C and Q (Fig. 7(e)). R_s, R_{ct}, Zw are ascribed to the series resistance, charge-transfer resistance and Warburg impedance, respectively. C is associated with the double layer capacitance and Q is correlated to the Faradic capacitance. EC-Lab V11.01 (ZSim-Bio-logic analysis) software was applied for the EIS data fitting.

The gravimetric specific capacitance (C_s, F g^{-1}) of electrodes was calculated from the galvanostatic discharge curves according to equation (1):

$$C_s = \frac{I\Delta t}{m\Delta V} \quad (1)$$

where, I is the discharge current (A), ΔV is discharging voltage, m is the mass of the active electrode material (g) and Δt is the discharge time. The volumetric capacitance (C_v, F/cm$^{3)}$ was calculated by the following equation:

$$C_v = \rho C_s \quad (2)$$

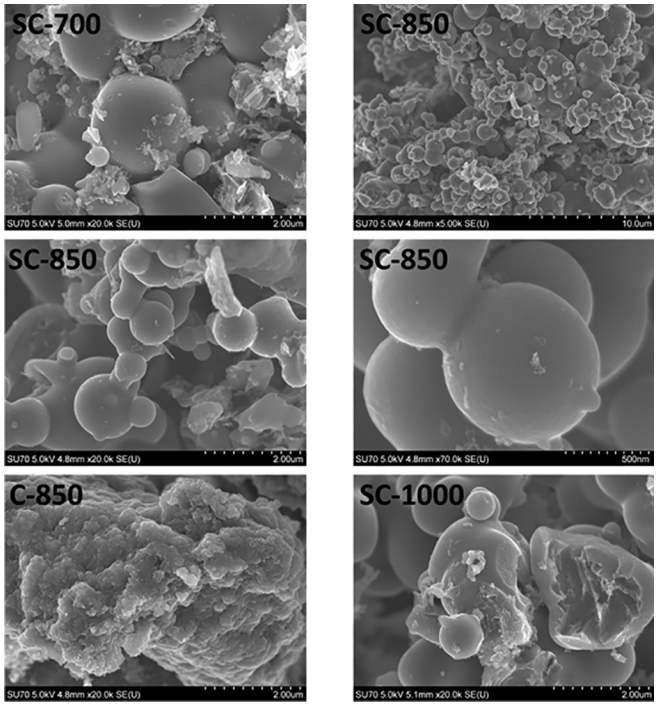

Fig. 3. SEM image of SC-700, SC-850 (variable magnification), C-850 and SC-1000.

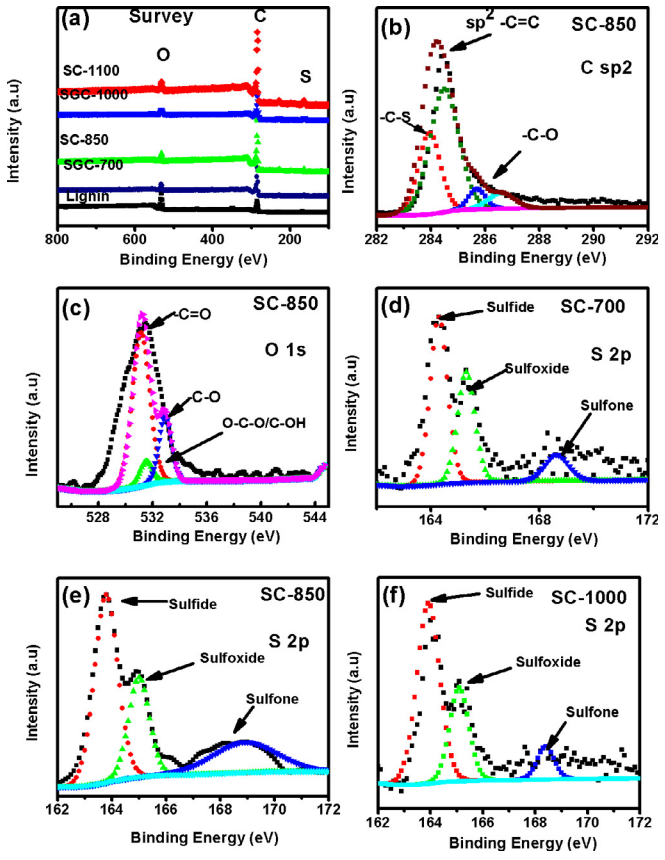

Fig. 4. XPS analysis of obtained materials (a) survey spectra of lignin, SC-700, SC-850 and SC-1000, (b) High resolution C 1s core level analysis of SC-850, (c) High resolution O 1s core level analysis of SC-850, (d) High resolution S *2p* core level analysis of SC-700, (e) High resolution S *2p* core level analysis of SC-850, (f) High resolution S *2p* core level analysis of SC-1000.

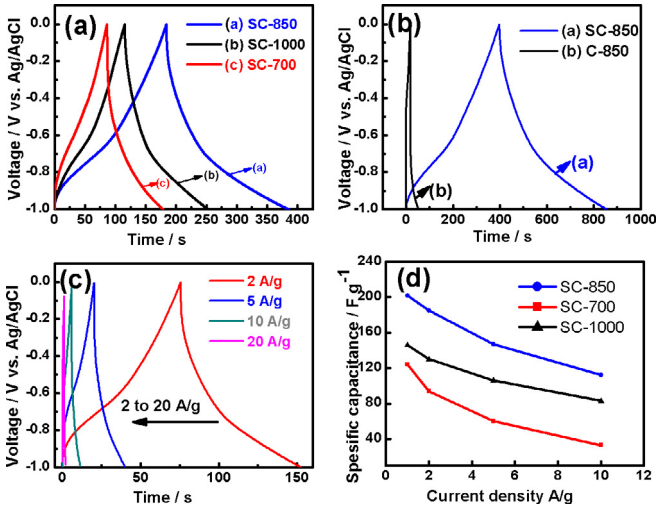

Fig. 5. (a) Charge-discharge curves of SC-700, SC-850 and SC-1000 at 1 A g^{-1}, (b) Charge-discharge curves of SC-850 and C-850 at 0.5 A. g^{-1}, (c) Charge-discharge curves of SC-850 at 2, 5, 10, 20 A g^{-1}, (d) Specific capacitance of obtained materials (all experiments were conducted in 1 M KOH electrolyte solution).

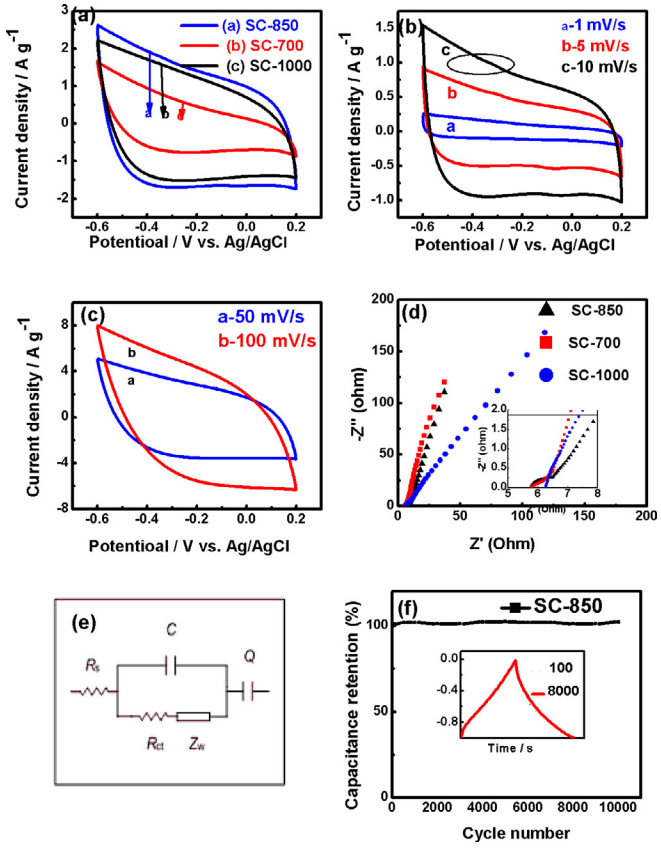

Fig. 6. (a) CV curves of SC-700, SC-850 and SC-1000 at 20 mV s^{-1} scan rate, (b) CV curves of SC-850 at scan rates of 1–10 mV s^{-1}, (c) CV curves of SC-850 at different scan rate from 50 to 100 mV s^{-1}, (d) Nyquist plot of SC-700, SC-850 and SC-1000, (e) electrical equivalent circuits (f) The cycling performance of SC-850 (all experiments were performed in 1 M KOH electrolyte solution).

where C_s is specific capacitance, ρ is particle density calculated by equation (3) [40,41]:

$$\rho = \frac{1}{V_t + \left(1/\rho_t\right)} \tag{3}$$

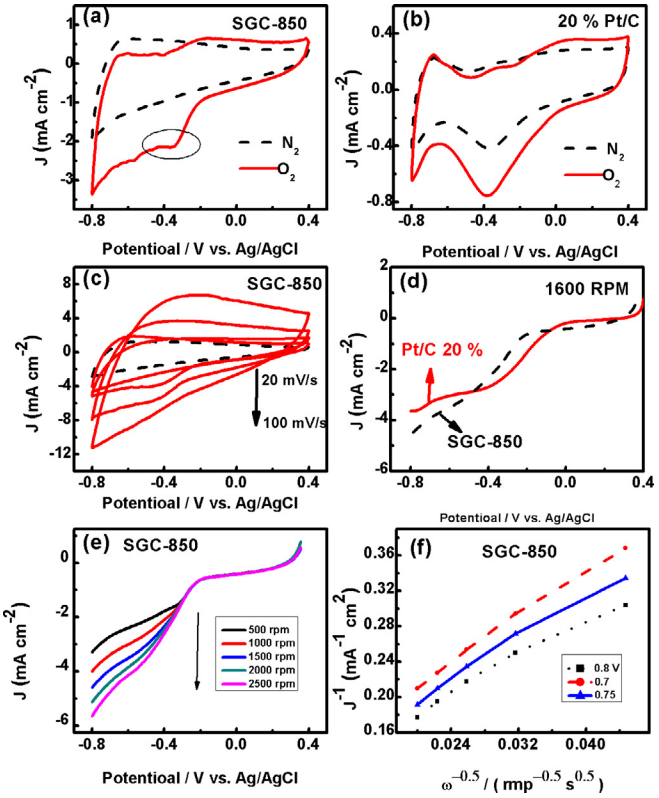

Fig. 7. CV curves of (a) SC-850 (b) 20 wt% Pt/C in N_2/O_2-saturated 0.1 M KOH electrolyte at 10 mV s^{-1} scan rate, (c) CV curve of SC-850 in N_2/O_2-saturated 0.1 M KOH electrolyte at variable scan rate, (d) RDE voltammograms for SC-850 and 20 wt% Pt/C in O_2-saturated 0.1 M KOH electrolyte rotation speed of 1600 rpm, (e) RDE voltammograms in O_2-saturated 0.1 M KOH electrolyte (rotation speed from 500 to 2500 rpm, sweep rate 5 mV s^{-1}), and (e) K–L plots derived from the RDE measurements at the potential between −0.6 and −0.8 V.

V_t is total pore volume cm [3]/g and ρ_t is true density of carbon (2 g/cm^3).

For the ORR measurements, the working electrode was prepared from an ink solution composed of 5 mg active material, 100 μL Nafion binder and 300 μL ethanol. The mixture was sonicated for 30 min and 8 μL of the resulting ink were dropped onto a freshly cleaned rotating disc glassy carbon electrode (RDE, 3 mm diameter, CH Instruments Inc.). The prepared RDE was warmed to 70 °C to improve adhesion of the active material on the glassy carbon electrode surface. 0.1 M (80 mL) KOH solution was used as an electrolyte in a three-electrode cell with RDE. The obtained current was normalized by the geometric area of the active surface (mA/m^2). For kinetic measurement, the Koutecky-Levich equation (4) was applied at the potential from 0.4 and −0.8 V and for rotational speed range from 500 to 2500 rpm as follows [42].

$$\frac{1}{J} = \frac{1}{J_k} + \frac{1}{B\omega^{0.5}} \tag{4}$$

where J is the current density, J_k is kinetic current density, ω was rotational speed, and B is the slope of K-L curve. The theoretical value of n can be calculated from the following equation (5):

$$B = 0.2nF\left(D_{O_2}\right)^{2/3} C_{O_2} v^{-1/6} \tag{5}$$

where, n is the number of electrons transferred per O_2 molecule during the oxygen reduction reaction, B is the slope of K-L curve, F is the faraday constant (96,485 C mol^{-1}), D_{O_2} (1.9 × 10 − 5 cm^2 s^{-1}) is the diffusion coefficient of O_2 in KOH electrolyte, C_{O_2} (1.2*10^{-6}) is concentration of O_2 in the electrolyte and ν (0.01 cm^2 s^{-1}) is the kinematic viscosity of the electrolyte.

Table 1
Elemental and surface chemical composition of sulfur self-doped materials by XPS analysis.

Sample	C (wt. %)	O (wt. %)	S (wt.%)	Sulfide (at.%)	Sulfoxide (at.%)	Sulfone (at.%)
Lignin	56.9/ 36.8*	37.3/ 43.9*	6.6/3.4*	-	-	-
SC-700	87.5	9.2	3.2	51.8	24.7	23.4
SC-850	90.5	6.9	2.6	65.7	27.5	6.6
SC-1000	91.1	6.4	2.5	47.6	37.5	14.8

*Bulk analysis.

3. Results and discussion

3.1. Physical properties

The pathway for the synthesis of sulfur self-doped carbons is illustrated in Fig. 1. The production of S-doped carbons has been designed to be facile, inexpensive, environmentally friendly, and easy to scale-up. The as-prepared S-doped carbons were labeled as SC-*x*, where S denotes the sulfur self-doping, C refers to carbon and *x* refers to the carbonization temperature in °C. Carbon C-850 (pristine) was also synthesized by following the same procedure from sulfur-free (organosolv) lignin.

In this study, we used two types of lignin. First, Norlig A (calcium lignosulfonate) lignin which is separated from woody plants in H_2SO_4 solution to form black liquor and then, lignin was precipitated by the addition of lime (CaO) [32]. The elemental composition of Norlig A is 36.8 wt% C, 37.3 wt% O, 6.7 wt% S, and 2.5 wt% Ca as shown in Table 1. The presence of calcium and sulfur atoms enhances the electrochemical and surface activation properties of the as-prepared carbon materials, as discussed in following sections. Second, lignol (organosolv) is a lignin lacking sulfur and calcium atoms in its structure due to the use of organic solvents in the separation process [32,43]. Organosolv lignin contains 65.4 wt% C and 35.6 wt% O. Absence of sulfur and calcium atoms in the organosolv lignin limits the electrochemical and surface activation properties in the resulting carbon material (C-850). It is important to point out that both the carbons surface activation by calcium and sulfur doping were carried out in-situ and in a one-step synthesis process via the careful design of the experiment and proper selection of the reaction precursors.

TGA was used to investigate the thermal decomposition of lignin, bio-char and the as-prepared sulfur self-doped carbon materials as shown in Fig. 2(a). Lignin, bio-char and SC-850 desorb water at 150 °C. Lignin started to decompose at 200 °C and continued the decomposition up to 725 °C. The residual ash content of lignin is calculated to be 16 wt % at 1000 °C. Approximately 41 wt% of bio-char remains at 850 °C as shown in Fig. 2(a). The TGA of the as-prepared SC-850 reflects its high thermal stability.

Lignin, bio-char and sulfur self-doped carbons were analyzed by FTIR in order to determine the transformation of the functional groups over the course of the synthesis process. The collected FTIR spectra are shown in Fig. 2(b). Several functional groups characteristic of the lignin structure are observed. For instance, the IR peaks located at 1032, 1420, 1450, 1507, and 1593 cm^{-1} correspond to the C-H bonds and aromatic ring groups of lignin. The peak located at 2939 cm^{-1} is ascribed to the vibration of the C-H bond from the aliphatic carbon in the lignin structure [33,36]. The –OH functional group of lignin displayed a peak around 3300 cm^{-1}. The characteristic IR peaks of lignin such as the –OH group disappeared in the IR spectra of the corresponding bio-char and carbon due to elimination of the hydroxyl groups during the HTC and thermal annealing steps [44].

Raman spectroscopy is a crucial technique to investigate the degree of graphitization for carbon materials. Fig. 2(c) displays two characteristic peaks in Raman spectra of the samples. The G band located at 1580 cm^{-1} corresponds to the graphitic carbon (sp^2) structure while the D band at 1360 cm^{-1} is associated with the disordered structure of the carbon-based materials [45]. The appearance of G and D bands in Raman spectra of the as-prepared sulfur self-doped carbons indicates that the structure consists of a combination of graphitic and disordered (amorphous) carbons. The intensity ratio of the D band (I_D) to G band (I_G) is an indicator of the formation of graphitization and disordered structure [46,47]. The lower I_D/I_G ratio corresponds to higher degree of graphitization in the resulting materials. The I_D/I_G ratios were found to be 0.83, 0.89, 0.97 and 1.01 for the SC-700, SC-850, SC-1000 and C-850, respectively confirms a high degree of graphitization. The slight enhancement in the I_D/I_G ratio at 850 and 1000 °C might be attributed to destruction of well ordered-graphitic structures at the higher annealing temperatures [48]. It is assumed that the specific capacitance of a carbon-based material increases with the amorphous carbon content due to the large surface area of the disordered structure. However, the electrical conductivity of amorphous carbon is low. On the other side, graphitic carbon possesses an outstanding electrical conductivity because of its well-ordered crystalline structure however, its surface area and pore size distribution is limited [46]. Thus, optimization of the graphitic/amorphous structural ratio in the carbon materials is crucial to obtain the desired electrochemical activity. In the present study, the carbon sample SG850 with I_D/I_G ratio of 0.89 displayed the highest electrochemical activity.

The N_2 adsorption/desorption isotherms and pore sizes distribution of the sulfur self-doped carbons are presented in Fig. 2(d and e). The BET surface area of the SC-700, SC-850, SC-1000, and C-850 were found to be 78, 660, 260, and < 20 m^2/g, respectively, as listed in Table 2. The total pore volume of SC-700, SC-850 and SC-1000 were found to be 0.05, 0.25 and 0.12 cc/g, respectively. It is worthwhile to mention that in the studied system, the surface area and pore sizes distribution of the as-prepared carbon samples are significantly influenced by the annealing temperature. The annealing temperature 850 °C was found to be the optimum temperature to produce carbon with high BET surface area. At the lower annealing temperature (700 °C), surface activation was not completed due to the insufficient thermal energy. The lower BET surface area of the SC-1000 sample is caused by collapsing of the micro/meso pores at the high annealing temperature [49,50]. We further compared the BET surface area of SC-850 with respect to C-850 (calcium free lignin). The surface area of C-850 (< 20 m^2/g) is significantly lower than that of SC-850. It is important to point out the synthetic strategy of both C-850 and SC-850 did not include any surface activation steps. As it mentioned in the previous sections, the carbon material derived from the organosolv lignin is calcium-free while the carbon materials derived from the calcium lignosulfonate lignin displayed up to 2.5 wt% calcium content. The high

Table 2
The capacitance, I_D/I_G ratio, S/C ratio, the BET surface area and pore volume values of the as-prepared carbon materials.

Sample	Capacitance (F/g)[a]	ID/IG	S/C ratio	BET surface area (m2/g)[b]	Micropore volume (cc/g)[c]	Total volume (cc/g)[d]
SC-700	124	0.83	0.0036	78	0.03(60)	0.05
SC-850	202	0.89	0.0028	660	0.19(76)	0.25
SC-1000	146	0.97	0.0027	260	0.08(67)	0.12
C-850	44	1.01		< 20		

[a] Calculated at 1 A/g current density except for C-850 at 0.5 A/g.
[b] BET surface area was calculated in the partial pressure range which gives the best linear fitting.
[c] Determined by cumulative pore volume at 2 nm maxima of the PSD assuming slit/cylindrical shaped pores and QSDFT model; the values in parentheses are the percentage of micropores volume relative to total pore volume.
[d] Total pore volume at P/Po = 0.95.

BET surface area of SC-850 reflects that the importance of calcium ions which act as a surface activating agent during the annealing treatment. This observation is in accordance with our previous finding that metal ions such as Mn^{2+} and Fe^{3+} can effectively activate the carbon surface [51]. The pore sizes distribution of the as-prepared carbon samples indicates their micro/meso porous nature as shown in Fig. 2(e). For example, the SC-850 sample displayed micropores of 1.5 nm and mesopore of 15 nm.

The SEM micrographs of the synthesized sulfur self-doped carbon materials are presented in Fig. 3. All the sulfur self-doped carbon samples displayed a similar morphology composed of spherical shaped particles that stick to each other in a random fashion with a size ranging from 0.5 to 3 μm. The main dissimilarity in the samples morphology was the size of the carbon spheres. The morphology of C-850 is different from SC-850 where microstructure of the C-850 is non-porous due to the absence of the surface activating catalyst/calcium ions and consists of fused carbon spheres that form a compact structure.

The surface chemical composition of sulfur self-doped carbons materials were investigated by means of X-ray photoelectron spectroscopy (XPS). The surface elemental composition and the corresponding functional groups of the prepared carbons are listed in Table 1. The survey scans of the sulfur self-doped carbon materials are shown in Fig. 4 (a). Carbon, oxygen, and sulfur peaks are located at 288.4, 532 and 164.7 eV, respectively. The carbon content has been significantly increased during the HTC and annealing processes to be ~1.6 times higher than that in the pure lignin as shown in Table 1. The observed enhancement in the carbon content of S-doped carbons reflects the efficiency of the carbonization process and could be attributed to the low volatility of the carbon compounds compared to those of the dopant such as oxygen and sulfur. In particular, the oxygen content has been significantly decreased through the HTC and thermal annealing steps being 5 to 6 times less than its value before the treatment, due to the deoxygenation of many functional groups (e.g., hydroxyl and carboxyl groups) which is consistent with FTIR results [52]. The S/C ratio is slightly decreased with the increase of the annealing temperature due to the volatility of sulfur compounds. The bulk elemental composition of lignin was compared with surface composition XPS data (e.g. 5–10 nm) as shown in Table 1. The variation between the XPS and bulk elemental analysis results arises from the fact that XPS is a surface sensitive technique that determine the surface composition of the materials (e.g. 5–10 nm), while C/H/S elemental analysis examines the bulk composition [53]. The C *1s*, O 1s and S *2p* high-resolution core-level spectra of the as-prepared carbon samples are depicted in Fig. 4. For XPS deconvolution of the C *1s,* the main peak located at 284.4 eV in Fig. 4(b) is attributed to the C=C group. The two small overlapped peaks observed at 285.6 eV and 286.5 eV are attributed to C-O, C=O and O-C=O functional groups [54]. Another peak located at 283.9 eV is assigned to C-S groups [55,56], which is consistent with the high-resolution core-level sulfur spectrum. The high-resolution XPS core-level scan of the O *1s* is presented in Fig. 4(c). Three types of oxygen functional groups can be identified from the spectrum. The main peak located at 531.2 eV refers to the C=O bond while the small peaks at 531.5 and 532.9 eV correspond to O-CO/C-OH bonds [57]. Careful examination of the S *2p* high-resolution core-level spectra indicates the presence of three types of sulfur functional groups as shown in Fig. 4 (d, e, f). The two core peaks located at 164 and 165.2 eV are assigned to sulfide (-S-C-S) and sulfoxide groups [27,45]. The relatively small peak seen at higher energy 168.6 eV is ascribed to -C-SO_2-C bonds (sulfone bridge) [55,58]. The effect of variable sulfur functional groups is discussed in the electrochemical results (see below).

3.2. Electrochemical capacitance

The galvanostatic charge/discharge (GCD) measurements were conducted in a three-electrode configuration to evaluate the electrochemical performance of the sulfur self-doped carbons as electrode material in supercapacitors. As shown in Fig. 5(a), all the sulfur self-doped carbons displayed nearly isosceles triangular-shaped GCD curves. Furthermore, the GCD measurements were performed at variable current densities of 5–20,000 mA/g. The SC-850 maintained the desired triangular-shaped even at higher current densities (up to 10 A/g) indicates a near ideal EDLC behavior with a fast charge propagation [14,45]. The specific capacitance (C_s, F/g) of the sulfur self-doped carbons was calculated from equation (1). The C_s for SC-700, SC-850 and SC-1000 are 124, 202 and 146 F g^{-1}, respectively at a current density of 1 A g^{-1} in 1 M KOH electrolyte. Although SC-700 displayed the highest sulfur surface content as indicated by the XPS data, its C_s is lower than that of SC-850 which is 1.6 times greater than the SC-700. The high C_s of SC-850 sample could be attributed to its high surface area (660 m^2/g) which is 8 times higher than that of SC-700 sample. The high surface area in conjunction with the enhanced pore volume facilitate mass transport of electrolyte through the pores of the electrode and provide more active sites for the electrosorption of electrolyte ions. Another factor that may contribute to the observed high capacitance of the SC-850 samples the higher amorphous carbon content. The SC-850 sample displayed higher I_D/I_G ratio than that of the SC-700 sample as shown in Table 2. It is already addressed before that amorphous carbon is assumed to possess large specific capacitance value while the graphitic carbon exhibits more conductivity [46]. Although the C_s of SC-700 is the lowest among the sulfur doped samples, the conductivity of the SC700 is higher than others. This finding is consistent with the EIS data and will be discussed in a more detail. The higher capacitance of SC-850 with respect to SC-1000 is associated with the synergistic effect of higher surface area, larger micropore volume and higher S/C ratio of the SC-850 sample. Moreover, the C_s of the SC-850 (225 F/g at 0.5 A/g) is about 5 times that of the un-doped C-850 (pristine) which was found to be 44 F/g at 0.5 A/g. The high C_s for the SC-850 could be attributed the presence of sulfur atoms (pseudocapacitance) which contribute to facilitate/improve the ion transport and increase the number of the electroactive centers/higher surface area. The proposed faradaic reaction of sulfur-containing functional groups was reported previously as follow [59].

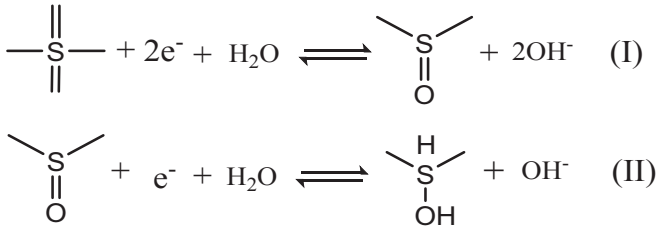

The faradaic reactions are originating from the sulfone and sulfoxide functional groups, respectively. In addition, the sulfide functional groups are responsible for enhancing the charge transfer at the sample surface. The sulfide functionalities could induce polarization of carbon surface via the interaction between the electron-rich sulfide groups and the carbon structure [59]. In the present study, the sulfur in the SC-850 is in the forms of 65.7% sulfide, 27.5% sulfoxide and 6.6% sulfone functional groups as revealed by the XPS data analysis. At variable current densities, the gravimetric specific capacitances of the SC-850 sample were found to be 185, 147, and 95 F/g at 2, 5 and 10 A/g, respectively. The outstanding performance even at higher current densities offering a good rate of capability [60]. The volumetric specific capacitances of SC-850 at variable current densities were calculated from equation (3) to be 300, 269, and 195 F/cm [3] at 0.5, 1 and 10 A/g current densities, respectively. Comparing the specific and volumetric capacitance values of SC-850 electrode with the literature [61–68] indicted that the specific and volumetric capacitance of SC-850 (225 F/g and 300 F/cm [3] at 0.5 A/g) are higher or comparable to the reported capacitance values for many biomass-based carbon electrodes [69–72].

To examine the presence of the pseudocapacitive contribution in the

as-prepared sulfur self-doped carbon materials, cyclic voltammetry measurements were also performed at variable scan rates. The CV data of the sulfur self-doped carbons revealed that SC-850 has the highest CV area, which is consistent with the galvanostatic charge/discharge measurements. The SC-850 sample displayed a nearly perfect rectangular shaped CV curve at 20 mV s^{-1} scan rate as shown in Fig. 6(a) which reflects an ideal double layer capacitor behavior. Close examination of the SC-850 sample's CVs at slow scan rates indicated the presence of pseudocapacitive behavior where redox peaks appeared around −0.3 V as depicted in Fig. 6(b). This peak could be attributed to the reversible faradaic redox reaction of the sulfone and sulfoxide surface functionalities [27,45]. The increased electrical resistance and poor penetration of the electrolyte into the electrode material pores at fast scan rates could account for the observed slight distortion of the CVs of the SC-850 sample from the rectangular shape, Fig. 6(c).

EIS measurements were conducted to examine the interfacial properties and electron transfer kinetics of the as-prepared sulfur self-doped carbon materials. Nyquist plots of the materials are presented in Fig. 6(d). They are similar, consisting of a semicircular part in the high frequency region and a linear part in the low frequency region. In the high frequency region, the intercept of the semicircular part of the Nyquist plot with the real impedance axis (Z′-real axis) gives the equivalent series resistance (ESR). For an electrochemical capacitor, the ESR governs the rate of the charged–discharge process and it is a combined resistance from the electrolyte ionic resistance, intrinsic and contact resistances of the current collector and the electrode material. The SC-700 and SC-850 electrodes displayed almost the same ESR of ~5.7 Ω as shown in Fig. 6(d). The observed relatively high resistance (6.3 Ω) for the SC-1000 electrode with respect to the other electrodes could be attributed to the poor accessibility of the electrolyte to the electrode material which resulted in slow electron and ion transfer rates. In the high-frequency region, the diameter of the semicircular part of the Nyquist plot gives the charge transfer resistance (R_{ct}) which originates from the electron transfer process (e.g. Faradic reactions) at the electrode surface. The SC-700 sample displayed smaller R_{ct} value (0.5 Ω) than that of the SC-850 sample (0.7 Ω). This slight variation in the conductivity might be assigned to the presence of higher degree of graphitization carbon content in the SC-700 than the SC-850. These findings are in agreement with the Raman data which indicated that the SC-700 has the lowest I_D/I_G ratio. In the low-frequency region, the linear part of the Nyquist plot for the SC-850 sample is obviously more vertical than that for the other sulfur self-doped materials, which is indicative of lower ionic diffusion resistance and so enhanced capacitive performance and faster ionic diffusion through the electrode material facilitated by its high surface area and porous nature.

It is important to test the cycling degradation of the supercapacitor electrode materials. The SC-850 sample displayed excellent cycling stability after 10,000 cycles at 5 A/g with a retention of specific capacitance close to 99% as displayed in Fig. 6 (e). Interestingly, the specific capacitance slightly increased during the charge-discharge cycling as shown in Fig. 6(a). This increase is due to physical opening of the clogged pores upon cycling [73]. The long cycle life of the tested electrodes reflects the reversibility of the Faradic redox process and high chemical and structural stability of the sulfur self-doped carbons, which make them potential candidates as a highly stable electrode material for supercapacitors.

3.3. Oxygen reduction reaction

We further investigated the application of the sulfur self-doped carbons as a potential ORR electrocatalyst. The SC-850 sample is chosen as a model example for the ORR study due to its superior performance as a supercapacitor electrode material. For comparison, commercial 20 wt % Pt/C catalyst was tested under the same conditions. The CV and linear sweep voltammetry (LSV) measurements were conducted in O_2 or N_2 saturated 0.1 M KOH aqueous electrolyte in order to assess the electrocatalytic activity of the SC-850 sample toward the ORR. As can be seen in Fig. 7(a), the collected CV curves at SC-850 as a working electrode material within the potential window +0.4 to −0.8 V in O_2-saturated 0.1 M KOH solution, exhibited well-defined oxygen cathodic reduction peaks centered around −0.33 V while the CV recorded in N_2- saturated 0.1 M KOH solution did not display any characteristic redox peaks (i.e., is featureless). The observed enhancement in the CV area demonstrates the high electrochemical activity of the SC-850 towards the oxygen reduction reaction. This is explained by the fact that sulfur doping provides extra catalytic sites for the ORR and ensures efficient electrolyte ion migration and electron transport. In addition, it is well known that the ad-atom in the N-doped carbons is predominantly responsible for enhancing the carbons ORR catalytic activity via changing the charge density around the carbon atom and make it more positive due to the higher electronegativity of N with respect to carbon. Such change in the charge density around the carbon atoms is unlikely to occur in the studied system (SC-850) due to the close electronegativity values of C (2.55) and S (2.58) atoms. As a result, the well-defined redox cathodic peak in the CV of the S-doped carbon sample could be attributed to the tailor spin density in the C-S bond as it reported before by Huang et al. [10] In order to compare the CV plot of SC-850 with that of the commercially available Pt/C catalyst, the CV plot of 20 wt% Pt/C was recorded under the same conditions as shown in Fig. 7 (b). The area under the CV curve of the commercial Pt/C catalyst is enhanced in the O_2 saturated electrolyte with respect to that obtained in the N_2 saturated electrolyte, and a characteristic oxygen reduction peak was observed around −0.37 V. The ORR peak for the SC-850 sample appeared at a more positive potential with respect to that recorded on the commercial Pt/C catalyst. In addition to the CV measurements, a LSV experiment was also carried out on rotational glassy carbon disk electrode at speeds from 500 to 2500 rpm within a potential range from 0.4 to −0.8 V at 5 mV s^{-1} scan rate. The LSV response of the SC-850 and Pt/C 20 wt% at 5 mV s^{-1} scan rate is shown in Fig. 7(d and e). The onset potentials are observed to be −0.17 and −0.06 V (vs. Ag/AgCl) for the SC-850 and Pt/C, respectively. The SC-850 sample displayed a comparable limiting current to the Pt/C catalyst at potential of −0.45 V and higher limiting current at a more negative potential. This finding indicates that the SC-850 sample has an excellent ORR activity. The current density is directly proportional to rotational speed and the corresponding K-L curve shows good linearity between J^{-1} and the inverse of square root of rotational speed which indicates a first-order reaction kinetics toward O_2 reduction (Fig. 7(f)) [74]. Four-electron pathway for reducing O_2 is highly desirable to obtain optimum energy capacity for the ORR applications and to avoid hydrogen peroxide formation, which is poisonous to the catalyst, as an intermediate. The number of electrons transferred per O_2 during the oxygen reduction reaction was calculated from Equations (4) and (5). The transferred electron number (n) is calculated to be 3.4 to 2.7 within the potential window −0.8 to −0.7 mV, respectively, which implies a four-electron oxygen reduction reaction. As previously reported, owing to asymmetric atomic spin density between carbon and sulfur atoms, the resulting doped structure provides extra active sites for O_2 surface adsorption [75]. These favorable active sites for diatomic adsorption could efficiently weaken O-O bonding and facilitate the direct reduction of oxygen into OH^- via a four-electron process [76].

4. Conclusions

In this work, we have shown that sulfur self-doped carbon materials were successfully synthesized from commercially available lignin via hydrothermal carbonization followed by thermal annealing. A facile, inexpensive and environmentally benign synthesis pathway has been developed. The as-prepared SC-850 sample exhibits high BET surface area of 660 m^2/g with abundant micro/meso porous structure. The SC-850 demonstrates an excellent capacitive behavior of 225 F/g at 0.5 A/g current density in 1.0 M KOH and high durability up to 10,000 cycles

at a harsh condition of 5 A/g current density. Furthermore, the SC-850 displayed a high electrocatalytic activity toward the ORR process in 0.1 M KOH electrolyte. In conclusion, the inexpensive and sustainable byproduct lignin has been easily converted into porous carbon, and the obtained material can further be utilized for energy storage and electrocatalysis applications.

Acknowledgement

Muslum Demir thanks the Ministry of National Educational of the Republic of Turkey for his graduate fellowship.

References

[1] P. Simon, Y. Gogotsi, Materials for electrochemical capacitors, Nat. Mater. 7 (11) (2008) 845–854.
[2] M.F. El-Kady, Y. Shao, R.B. Kaner, Graphene for batteries, supercapacitors and beyond, Nat. Rev. Mater. 1 (2016) 16033.
[3] H. Luo, Z. Liu, L. Chao, X. Wu, X. Lei, Z. Chang, X. Sun, Synthesis of hierarchical porous N-doped sandwich-type carbon composites as high-performance supercapacitor electrodes, J. Mater. Chem. 3 (7) (2015) 3667–3675.
[4] G. Wang, L. Zhang, J. Zhang, A review of electrode materials for electrochemical supercapacitors, Chem. Soc. Rev. 41 (2) (2012) 797–828.
[5] M. Zhi, C. Xiang, J. Li, M. Li, N. Wu, Nanostructured carbon–metal oxide composite electrodes for supercapacitors: a review, Nanoscale 5 (1) (2013) 72–88.
[6] T.Y. Wei, X.L. Wei, Y. Gao, H.M. Li, Large scale production of biomass-derived nitrogen-doped porous carbon materials for supercapacitors, Electrochim. Acta 169 (2015) 186–194.
[7] C.Q. Yuan, X.H. Liu, M.Y. Jia, Z.X. Luo, J.N. Yao, Facile preparation of N- and O-doped hollow carbon spheres derived from poly(o-phenylenediamine) for supercapacitors, J. Mater. Chem. 3 (7) (2015) 3409–3415.
[8] M. Demir, B. Ashourirad, J.H. Mugumya, S.K. Saraswat, H.M. El-Kaderi, R.B. Gupta, Nitrogen and oxygen dual-doped porous carbons prepared from pea protein as electrode materials for high performance supercapacitors, Int. J. Hydrogen Energy (2018) ISSN 0360-3199 https://doi.org/10.1016/j.ijhydene.2018.03.220.
[9] M. Demir, T.D. Tessema, A.A. Farghaly, E. Nyankson, S.K. Saraswat, B. Aksoy, R.B. Gupta, Lignin-derived heteroatom-doped porous carbons for supercapacitor and CO2 capture applications, Int. J. Energy Res. (2018) 1–15 https://doi.org/10.1002/er.4058.
[10] B. Ashourirad, M. Demir, R.A. Smith, R.B. Gupta, H.M. El-Kaderi, Rapid transformation of heterocyclic building blocks into nanoporous carbons for high-performance supercapacitors, RSC Adv. 8 (22) (2018) 12300–12309.
[11] D.T. Dam, T. Huang, J.-M. Lee, Ultra-small and low crystalline CoMoO 4 nanorods for electrochemical capacitors, Sustainable Energy Fuels 1 (2) (2017) 324–335.
[12] M. Demir, S.K. Saraswat, R.B. Gupta, Hierarchical nitrogen-doped porous carbon derived from lecithin for high-performance supercapacitors, RSC Adv. 7 (67) (2017) 42430–42442.
[13] L.L. Zhang, X.S. Zhao, Carbon-based materials as supercapacitor electrodes, Chem. Soc. Rev. 38 (9) (2009) 2520–2531.
[14] X. Chen, X.H. Chen, X. Xu, Z. Yang, Z. Liu, L.J. Zhang, X.J. Xu, Y. Chen, S.M. Huang, Sulfur-doped porous reduced graphene oxide hollow nanosphere frameworks as metal-free electrocatalysts for oxygen reduction reaction and as supercapacitor electrode materials, Nanoscale 6 (22) (2014) 13740–13747.
[15] Xi'an Chen, et al., Sulfur-doped porous reduced graphene oxide hollow nanosphere frameworks as metal-free electrocatalysts for oxygen reduction reaction and as supercapacitor electrode materials, Nanoscale 6.22 (2014) 13740–13747.
[16] W. Kiciński, M. Szala, M. Bystrzejewski, Sulfur-doped porous carbons: synthesis and applications, Carbon 68 (2014) 1–32.
[17] D.Y. Zhang, Y. Hao, L.W. Zheng, Y. Ma, H.X. Feng, H.M. Luo, Nitrogen and sulfur co-doped ordered mesoporous carbon with enhanced electrochemical capacitance performance, J. Mater. Chem. 1 (26) (2013) 7584–7591.
[18] J.P. Paraknowitsch, A. Thomas, Doping carbons beyond nitrogen: an overview of advanced heteroatom doped carbons with boron, sulphur and phosphorus for energy applications, Energy Environ. Sci. 6 (10) (2013) 2839–2855.
[19] G.A. Ferrero, M. Sevilla, A.B. Fuertes, Free-standing hybrid films based on graphene and porous carbon particles for flexible supercapacitors, Sustainable Energy Fuels 1 (1) (2017) 127–137.
[20] P. Chen, L.K. Wang, G. Wang, M.R. Gao, J. Ge, W.J. Yuan, Y.H. Shen, A.J. Xie, S.H. Yu, Nitrogen-doped nanoporous carbon nanosheets derived from plant biomass: an efficient catalyst for oxygen reduction reaction, Energy Environ. Sci. 7 (12) (2014) 4095–4103.
[21] X.J. Liu, Y.C. Zhou, W.J. Zhou, L.G. Li, S.B. Huang, S.W. Chen, Biomass-derived nitrogen self-doped porous carbon as effective metal-free catalysts for oxygen reduction reaction, Nanoscale 7 (14) (2015) 6136–6142.
[22] N. Brun, S.A. Wohlgemuth, P. Osiceanu, M.M. Titirici, Original design of nitrogen-doped carbon aerogels from sustainable precursors: application as metal-free oxygen reduction catalysts, Green Chem. 15 (9) (2013) 2514–2524.
[23] R. Bashyam, P. Zelenay, A class of non-precious metal composite catalysts for fuel cells, Nature 443 (7107) (2006) 63–66.
[24] S.A. Wohlgemuth, R.J. White, M.G. Willinger, M.M. Titirici, M. Antonietti, A one-pot hydrothermal synthesis of sulfur and nitrogen doped carbon aerogels with enhanced electrocatalytic activity in the oxygen reduction reaction, Green Chem. 14 (5) (2012) 1515–1523.
[25] X. Yu, S.K. Park, S.H. Yeon, H.S. Park, Three-dimensional, sulfur-incorporated graphene aerogels for the enhanced performances of pseudocapacitive electrodes, J. Power Sources 278 (2015) 484–489.
[26] J. Cai, H. Niu, Z. Li, Y. Du, P. Cizek, Z. Xie, H. Xiong, T. Lin, High-performance supercapacitor electrode materials from cellulose-derived carbon nanofibers, ACS Appl. Mater. Interfaces 7 (27) (2015) 14946–14953.
[27] X. Zhao, Q. Zhang, C.-M. Chen, B. Zhang, S. Reiche, A. Wang, T. Zhang, R. Schlögl, D.S. Su, Aromatic sulfide, sulfoxide, and sulfone mediated mesoporous carbon monolith for use in supercapacitor, Nanomater. Energy 1 (4) (2012) 624–630.
[28] J. Deng, M. Li, Y. Wang, Biomass-derived carbon: synthesis and applications in energy storage and conversion, Green Chem. 18 (18) (2016) 4824–4854.
[29] W.H. Yu, H.L. Wang, S. Liu, N. Mao, X. Liu, J. Shi, W. Liu, S.G. Chen, X.N. Wang, O-codoped hierarchical porous carbons derived from algae for high-capacity supercapacitors and battery anodes, J. Mater. Chem. 4 (16) (2016) 5973–5983.
[30] J.-W. Jeon, L. Zhang, J.L. Lutkenhaus, D.D. Laskar, J.P. Lemmon, D. Choi, M.I. Nandasiri, A. Hashmi, J. Xu, R.K. Motkuri, C.A. Fernandez, J. Liu, M.P. Tucker, P.B. McGrail, B. Yang, S.K. Nune, Controlling porosity in lignin-derived nanoporous carbon for supercapacitor applications, ChemSusChem 8 (3) (2015) 428–432.
[31] M. Graglia, J. Pampel, T. Hantke, T.-P. Fellinger, D. Esposito, Nitro lignin-derived nitrogen-doped carbon as an efficient and sustainable electrocatalyst for oxygen reduction, ACS Nano 10 (4) (2016) 4364–4371.
[32] J.D. Gargulak, S.E. Lebo, T.J. McNally, Lignin, Kirk-Othmer Encyclopedia of hemical Technology, John Wiley & Sons, Inc., 2000.
[33] C. Li, X. Zhao, A. Wang, G.W. Huber, T. Zhang, Catalytic transformation of lignin for the production of chemicals and fuels, Chem. Rev. 115 (21) (2015) 11559–11624.
[34] M. Fache, B. Boutevin, S. Caillol, Vanillin production from lignin and its use as a renewable chemical, ACS Sustain. Chem. Eng. 4 (1) (2015) 35–46.
[35] R. Katahira, A. Mittal, K. McKinney, X. Chen, M. Tucker, D.K. Johnson, G.T. Beckham, Base-catalyzed depolymerization of biorefinery lignins, ACS Sustain. Chem. Eng. 4 (3) (2016) 1474–1486.
[36] Q. Liu, S. Wang, Y. Zheng, Z. Luo, K. Cen, Mechanism study of wood lignin pyrolysis by using TG–FTIR analysis, J. Anal. Appl. Pyrol. 82 (1) (2008) 170–177.
[37] R. Demir-Cakan, N. Baccile, M. Antonietti, M.-M. Titirici, Carboxylate-rich carbonaceous materials via one-step hydrothermal carbonization of glucose in the presence of acrylic acid, Chem. Mater. 21 (3) (2009) 484–490.
[38] M. Gönen, E. Nyankson, R.B. Gupta, Boric acid production from colemanite together with ex situ CO2 sequestration, Indus. Eng. Chem. Res. 55 (17) (2016) 5116–5124.
[39] H. Ramsurn, S. Kumar, R.B. Gupta, Enhancement of biochar gasification in alkali hydrothermal medium by passivation of inorganic components using Ca (OH) 2, Energy Fuels 25 (5) (2011) 2389–2398.
[40] Q.X. Xie, R.R. Bao, A.R. Zheng, Y.F. Zhang, S.H. Wu, C. Xie, P. Zhao, Sustainable low-cost Green electrodes with high volumetric capacitance for aqueous symmetric supercapacitors with high energy density, ACS Sustain. Chem. Eng. 4 (3) (2016) 1422–1430.
[41] C.L. Long, L.L. Jiang, X.L. Wu, Y.T. Jiang, D.R. Yang, C.K. Wang, T. Wei, Z.J. Fan, Facile synthesis of functionalized porous carbon with three-dimensional interconnected pore structure for high volumetric performance supercapacitors, Carbon 93 (2015) 412–420.
[42] Z.C. Zuo, W. Li, A. Manthiram, N-heterocycles tethered graphene as efficient metal-free catalysts for an oxygen reduction reaction in fuel cells, J. Mater. Chem. 1 (35) (2013) 10166–10172.
[43] C.A. Mullen, A.A. Boateng, Catalytic pyrolysis-GC/MS of lignin from several sources, Fuel Process. Technol. 91 (11) (2010) 1446–1458.
[44] L. Wang, Y.L. Zheng, Q.Y. Zhang, L. Zuo, S.L. Chen, S.H. Chen, H.Q. Hou, Y.H. Song, Template-free synthesis of hierarchical porous carbon derived from low-cost biomass for high-performance supercapacitors, RSC Adv. 4 (93) (2014) 51072–51079.
[45] W.T. Gu, M. Sevilla, A. Magasinski, A.B. Fuertes, G. Yushin, Sulfur-containing activated carbons with greatly reduced content of bottle neck pores for double-layer capacitors: a case study for pseudocapacitance detection, Energy Environ. Sci. 6 (8) (2013) 2465–2476.
[46] M. Sevilla, R. Mokaya, Energy storage applications of activated carbons: supercapacitors and hydrogen storage, Energy Environ. Sci. 7 (4) (2014) 1250–1280.
[47] C.-h. Huang, R.-a. Doong, D. Gu, D. Zhao, Dual-template synthesis of magnetically-separable hierarchically-ordered porous carbons by catalytic graphitization, Carbon 49 (9) (2011) 3055–3064.
[48] M. Sevilla, A.B. Fuertes, Catalytic graphitization of templated mesoporous carbons, Carbon 44 (3) (2006) 468–474.
[49] G. Ma, Q. Yang, K. Sun, H. Peng, F. Ran, X. Zhao, Z. Lei, Nitrogen-doped porous carbon derived from biomass waste for high-performance supercapacitor, Bioresour. Technol. 197 (2015) 137–142.
[50] E. Fiset, J.-S. Bae, T.E. Rufford, S. Bhatia, G.Q. Lu, D. Hulicova-Jurcakova, Effects of structural properties of silicon carbide-derived carbons on their electrochemical double-layer capacitance in aqueous and organic electrolytes, J. Solid State Electrochem. 18 (3) (2013) 703–711.
[51] M. Demir, Z. Kahveci, B. Aksoy, N.K. Palapati, A. Subramanian, H.T. Cullinan, H.M. El-Kaderi, C.T. Harris, R.B. Gupta, Graphitic biocarbon from metal-catalyzed hydrothermal carbonization of lignin, Ind. Eng. Chem. Res. 54 (43) (2015) 10731–10739.
[52] G.-w. Sun, C. Wang, L. Zhan, W.-m. Qiao, X.-y. Liang, L.-c. Ling, Influence of high temperature treatment of activated carbon on performance of supercapacitors, Mater. Sci. Eng. 2 (2008) 41–48.
[53] D. Hulicova-Jurcakova, M. Seredych, G.Q. Lu, T.J. Bandosz, Combined effect of nitrogen-and oxygen-containing functional groups of microporous activated carbon

on its electrochemical performance in supercapacitors, Adv. Funct. Mater. 19 (3) (2009) 438–447.
[54] S. Gharehkhani, S.F.S. Shirazi, S.P. Jahromi, M. Sookhakian, S. Baradaran, H. Yarmand, A.A. Oshkour, S.N. Kazi, W.J. Basirun, Spongy nitrogen-doped activated carbonaceous hybrid derived from biomass material/graphene oxide for supercapacitor electrodes, RSC Adv. 5 (51) (2015) 40505–40513.
[55] W.I. Hayes, P. Joseph, M.Z. Mughal, P. Papakonstantinou, Production of reduced graphene oxide via hydrothermal reduction in an aqueous sulphuric acid suspension and its electrochemical behaviour, J. Solid State Electrochem. 19 (2) (2015) 361–380.
[56] J. Liang, Y. Jiao, M. Jaroniec, S.Z. Qiao, Sulfur and nitrogen dual-doped mesoporous graphene electrocatalyst for oxygen reduction with synergistically enhanced performance, Angew. Chem. Int. Ed. 51 (46) (2012) 11496–11500.
[57] L.H. Ai, X.M. Liu, J. Jiang, Synthesis of loofah sponge carbon supported bimetallic silver-cobalt nanoparticles with enhanced catalytic activity towards hydrogen generation from sodium borohydride hydrolysis, J. Alloy. Comp. 625 (2015) 164–170.
[58] J.P. Paraknowitsch, A. Thomas, J. Schmidt, Microporous sulfur-doped carbon from thienyl-based polymer network precursors, Chem. Commun. 47 (29) (2011) 8283–8285.
[59] X. Zhao, Q. Zhang, C.-M. Chen, B. Zhang, S. Reiche, A. Wang, T. Zhang, R. Schlögl, D.S. Su, Aromatic sulfide, sulfoxide, and sulfone mediated mesoporous carbon monolith for use in supercapacitor, Nanomater. Energy 1 (4) (2012) 624–630.
[60] Haobin Feng, Hang Hu, Hanwu Dong, Yong Xiao, Yijin Cai, Bingfu Lei, Yingliang Liu, Mingtao Zheng, Hierarchical structured carbon derived from bagasse wastes: a simple and efficient synthesis route and its improved electrochemical properties for high-performance supercapacitors, J. Power Sources 302 (2016) 164–173.
[61] F. Chen, W.J. Zhou, H.F. Yao, P. Fan, J.T. Yang, Z.D. Fei, M.Q. Zhong, Self-assembly of NiO nanoparticles in lignin-derived mesoporous carbons for supercapacitor applications, Green Chem. 15 (11) (2013) 3057–3063.
[62] K.L. Wang, Y.H. Cao, X.M. Wang, M.A. Castro, B. Luo, Z.R. Gu, J. Liu, J.D. Hoefelmeyer, Q.H. Fan, Rod-shape porous carbon derived from aniline modified lignin for symmetric supercapacitors, J. Power Sources 307 (2016) 462–467.
[63] S.X. Hu, S.L. Zhang, N. Pan, Y.L. Hsieh, High energy density supercapacitors from lignin derived submicron activated carbon fibers in aqueous electrolytes, J. Power Sources 270 (2014) 106–112.
[64] W.L. Zhang, M.Z. Zhao, R.Y. Liu, X.F. Wang, H.B. Lin, Hierarchical porous carbon derived from lignin for high performance supercapacitor, Colloid. Surface. 484 (2015) 518–527.
[65] F. Chen, Z. Zhou, L. Chang, T. Kuang, Z. Zhao, P. Fan, J. Yang, M. Zhong, Synthesis and characterization of lignosulfonate-derived hierarchical porous graphitic carbons for electrochemical performances, Microporous Mesoporous Mater. 247 (2017) 184–189.
[66] L. Zhu, Q. Gao, Y. Tan, W. Tian, J. Xu, K. Yang, C. Yang, Nitrogen and oxygen co-doped microporous carbons derived from the leaves of Euonymus japonicas as high performance supercapacitor electrode material, Microporous Mesoporous Mater. 210 (2015) 1–9.
[67] I.I.G. Inal, S.M. Holmes, A. Banford, Z. Aktas, The performance of supercapacitor electrodes developed from chemically activated carbon produced from waste tea, Appl. Surf. Sci. 357 (2015) 696–703.
[68] B.J. Jiang, C.G. Tian, L. Wang, L. Sun, C. Chen, X.Z. Nong, Y.J. Qiao, H.G. Fu, Highly concentrated, stable nitrogen-doped graphene for supercapacitors: simultaneous doping and reduction, Appl. Surf. Sci. 258 (8) (2012) 3438–3443.
[69] H. Li, D. Yuan, C.H. Tang, S.X. Wang, J.T. Sun, Z.B. Li, T. Tang, F.K. Wang, H. Gong, C.B. He, Lignin-derived interconnected hierarchical porous carbon monolith with large areal/volumetric capacitances for supercapacitor, Carbon 100 (2016) 151–157.
[70] D. Saha, Y.C. Li, Z.H. Bi, J.H. Chen, J.K. Keum, D.K. Hensley, H.A. Grappe, H.M. Meyer, S. Dai, M.P. Paranthaman, A.K. Naskar, Studies on supercapacitor electrode material from activated lignin-derived mesoporous carbon, Langmuir 30 (3) (2014) 900–910.
[71] H.B. Zhao, W.D. Wang, Q.F. Lu, T.T. Lin, Q.L. Lin, H.J. Yang, Preparation and application of porous nitrogen-doped graphene obtained by co-pyrolysis of lignosulfonate and graphene oxide, Bioresour. Technol. 176 (2015) 106–111.
[72] Y.W. Qiang, J.G. Jiang, Y.C. Xiong, H. Chen, J.Y. Chen, S.Y. Guan, J.D. Chen, Facile synthesis of N/P co-doped carbons with tailored hierarchically porous structures for supercapacitor applications, RSC Adv. 6 (12) (2016) 9772–9778.
[73] M. Lee, G.P. Kim, H.D. Song, S. Park, J. Yi, Preparation of energy storage material derived from a used cigarette filter for a supercapacitor electrode, Nanotechnology 25 (34) (2014).
[74] H. Zhang, J. Chen, Y. Li, P. Liu, Y. Wang, T. An, H. Zhao, Nitrogen-doped carbon nanodots@ nanospheres as an efficient electrocatalyst for oxygen reduction reaction, Electrochim. Acta 165 (2015) 7–13.
[75] Z. Yang, Z. Yao, G. Li, G. Fang, H. Nie, Z. Liu, X. Zhou, X.A. Chen, S. Huang, Sulfur-doped graphene as an efficient metal-free cathode catalyst for oxygen reduction, ACS Nano 6 (1) (2011) 205–211.
[76] J. Liang, Y. Jiao, M. Jaroniec, S.Z. Qiao, Sulfur and nitrogen dual-doped mesoporous graphene electrocatalyst for oxygen reduction with synergistically enhanced performance, Angew. Chem. Int. Ed. 2012 51 (46) (2012) 11496–11500.